

An enhanced bandwidth disturbance observer based control– S-filter approach

Mehmet Önder EFE^{1,*}, Coşku KASNAKOĞLU²

¹Department of Computer Engineering, Hacettepe University, Ankara, Turkey

²Department of Electrical and Electronics Engineering, TOBB University of Economics and Technology, Ankara, Turkey

Received: 03.09.2020

Accepted/Published Online: 16.02.2021

Final Version: 26.07.2021

Abstract: A continuous time enhanced bandwidth disturbance observer based control (DOBC) scheme is proposed in this paper. The classical Q -filter is implemented in feedback form and a signum function is inserted into the loop. The loop with this modification becomes capable of detecting small magnitude matched disturbances and we present an in depth discussion of the stability and performance issues comparatively. The proposed approach is called S-filter approach and the results outperform the classical approach under certain conditions. The contribution of the current paper is to advance the subject area to nonlinear filters for DOBC loops with guaranteed stability and performance. A specific case containing a signum function is elaborated throughout the paper and the obtained energy of the disturbance prediction error is shown to be smaller than the Q -filter based counterpart.

Key words: Disturbance observer, robust control, modified disturbance observer, enhanced bandwidth disturbance observer based control (DOBC), S-filter

1. Introduction

Disturbance observers (DOs) have been studied extensively in the past few decades and very important facts have been reported. Successful implementations of DOs have been reported and predicting the disturbances acting on the system input has become one of the interesting challenges for the control engineers.

Between 1989-2020, the number of outcomes with the keyword *disturbance observer* indexed by Web of Science increased approximately like $0.22(n - 1989)^{2-3}$, where n is the corresponding year. This observation is a clear indicator of how interesting the disturbance observers have been so far. Vast majority of the reported work contributed to the application side of DOs and some advanced the subject area by contributing to the theory. Current paper gives a new analysis and remodeling approach for the classical DO structure and proposes a modification that makes the obtained DO nonlinear yet sensitive to small magnitude disturbance signals entering through the control channel.

The notion of disturbance observer was introduced by the pioneering work of Prof. Kouhei Ohnishi, in 1983, [1]. Since then numerous strides have been made and, among them, the works by Sarıyıldız and his co-authors contributed mainly to the structure, stability, robustness, bandwidth, and the issues focusing around the functionality/limitations of disturbance observers rather than the applications, [2–7]. Cases concerning minimum phase plant, plant with time delay, plant with right half plane zero and unstable plant are studied and a set of bandwidth constraints are derived using Bode and Poisson integral formulas, [2]. Reaction torque

*Correspondence: onderefe@gmail.com

observer is introduced to remedy the noisy velocity measurements in motion control system, [3], and this necessitates the re-analysis of stability and performance issues keeping the bandwidth of the DO at the center. The work in [3] is further elaborated in [4], where a Lyapunov approach is developed for robot manipulators. The bandwidth constraints for the DO structure employing a first order lowpass filter is studied in [5], where the stability of the Kharitonov polynomials are scrutinized using Mikhailov criterion with the goal of relating robustness and bandwidth under parametric uncertainties. This is also considered in [6] with higher order lowpass filters with a performance versus trade-off discussion. The issues of time delay is considered in [7]. In [8], it is emphasized that the performance of DO gets better as the bandwidth of the lowpass filter gets larger yet this is a significant issue that provokes the undesired effects of noise on the closed loop performance. In all of the works in [2–6, 8], the used lowpass filter is a continuous and linear one, a typical choice is a first order transfer function. In [9], the problem of bandwidth selection is formulated as an optimization problem and a MATLAB (MathWorks, Inc., Natick, MA, USA) toolbox is introduced that minimizes the energy of the error over a set of bandwidth values.

The concept of DOBC has successfully been applied to mechanical systems, [10–13] and comprehensive surveys about the DOs can be found in [14–16]. In [17], an almost necessary and sufficient condition for robust stability of the closed loop is studied for a Q -filter that has sufficiently large time constant. The design of the Q -filter is performed via solving an optimization problem in [18], where the filter order is larger than one and a gradient search is performed for the iterative tuning purpose. In [19], 35 years of DOBC experience is reviewed and a useful list of relevant research outcomes is given.

Nonlinear versions of DO structures are reported in [20–22]. In [20], the DOBC approach is restructured with the notion of variable structure systems employing discontinuous functions, a natural consequence of which was emphasized as the sensitivity to noise. In [21], nonlinear DO is developed for nonlinear plant and the time derivative of the disturbance signal is assumed to be bounded as in the current paper. In [22], dead zone and saturation type nonlinear elements are utilized in the proposed scheme yet the Q -filter is considered as a linear lowpass filter.

Most recent applications of DOs utilizing continuous time, first (or higher) order Q -filter structure focus on DC-DC boost converters in [23], eliminating voltage fluctuations in power systems in [24], brushless DC motors in [25], assistive exoskeletons in [26], photoelectric stabilized platforms in [27], brushed DC motor control in [28] and ball balancer system in [29]. The cited volume of works use the Q -filter based architecture at various capacities and contributions.

The framework considering the discrete time conditions is presented in [30]. The discrete time case of [30] assumes a saturation function, where a finite gain around zero is a necessity; whereas, the current paper considers a signum function leading to a totally different theorem and proof. Further, the conclusions of the current paper are different from those of [30] in that the required bound for the 1-norm expressions are different. This work should therefore be viewed as a complementary work of [30] that guides the practicing engineers.

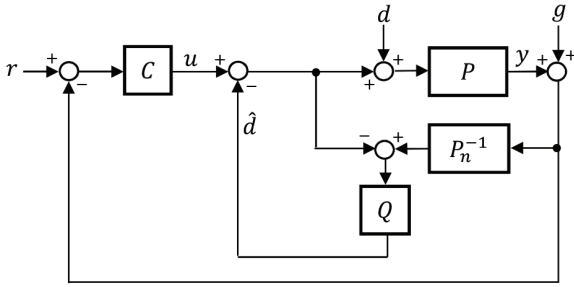
This paper is organized as follows: The second section presents an expansion of the Q -filter and derives the governing equations according to variables defined within this new scheme. Third section introduces the proposed modification and gives a discussion on stability and performance issues, as well as conditions related to a stability performance. The fourth section gives a comparative exemplar case where the energy content of the error signal is emphasized. The simulations compare the Q -filter approach and the proposed approach. The fifth section lists explicitly the contributions of the S-filter based DOBC and the concluding remarks are given

at the end of the paper.

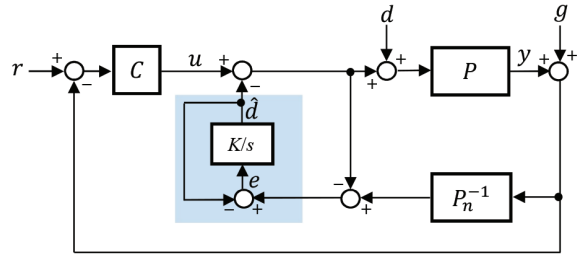
2. Expanding the Q -filter based DOBC structure

In Figure 1a, classical DOBC structure is depicted. In the shown block diagram P is the uncertain plant under control, P_n is the known nominal model of the plant P , C is the controller designed for the nominal plant model, Q is a lowpass filter, which is assumed as a first order one in this paper, i.e. $Q(s) = \frac{K}{s+K}$ with $K > 0$ is the parameter determining the bandwidth of the classical scheme. The system shown in Figure 1a, has three inputs, namely, the reference signal denoted by r , the unknown disturbance denoted by d , and the measurement noise denoted by g . The DOBC scheme predicts the value of d and outputs a signal \hat{d} , which is subtracted from the control signal path to compensate the deterioration caused by the disturbance d .

We redraw the block diagram in Figure 1a as in Figure 1b, where the first order filter, Q , is implemented in feedback form as shown in the shaded area of Figure 1b. Such an interpretation has been studied previously in [31] for discrete time implementations.



(a) Block diagram of the Q -filter based classical DOBC scheme.



(b) Expanded Q -filter based disturbance observer block diagram.

Figure 1. Classical block diagram and feedback realization of the Q filter.

Two fundamental equations can be derived from Figure 1b, and these equations are given as

$$u = \frac{C}{1 + PC}r - \frac{PC}{1 + PC}(d - \hat{d}) - \frac{C}{1 + PC}g \tag{1}$$

$$e = \frac{(PP_n^{-1} - 1)C}{1 + PC}r + \frac{PP_n^{-1} + PC}{1 + PC}(d - \hat{d}) + Ng \tag{2}$$

where $N := P_n^{-1} \frac{1+P_n C}{1+PC}$. Define the sensitivity transfer function as $S := \frac{1}{1+PC}$ and the complementary sensitivity transfer function as $T := 1 - S = \frac{PC}{1+PC}$. For the nominal closed loop system, we define $S_n := \frac{1}{1+P_n C}$ and $T_n := 1 - S_n = \frac{P_n C}{1+P_n C}$. Let $\Delta(s)$ denote an unknown transfer function such that $\|\Delta\|_\infty \leq 1$ and let W denote a transfer function, such that $\|W\|_\infty < \infty$.

The signal to the block with transfer function K/s in Figure 1b is denoted by e , and using (1) and (2), the general expression for e can be derived as in (3)

$$e = GCr + (1 + G)(d - \hat{d}) + Ng \tag{3}$$

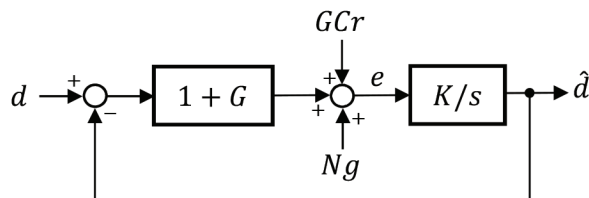
where the transfer function $G := \frac{PP^{-1}-1}{1+PC}$ is defined in the Table for four fundamental uncertainty types and it is independent of K . The fundamental assumption in this work is $G \in \mathcal{H}_\infty$ as we will be imposing conditions on the infinity norm and 1-norm of G .

According to Figure 1b, the quantity denoted by e passes through the block K/s and the obtained output is \hat{d} . A mathematically equivalent block diagram implementing (3) is illustrated in Figure 2a.

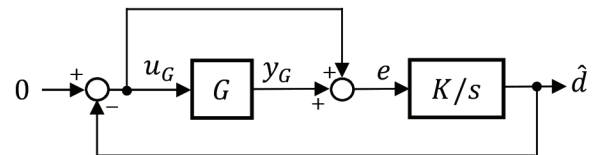
Table . Types of uncertainty and corresponding $G(s)$ expression

Uncertainty type	$G(s)$
$P = P_n(1 + \Delta W)$	$G(s) = \Delta W S$
$P = P_n + \Delta W$	$G(s) = P_n^{-1} \Delta W S$
$P = P_n / (1 + \Delta W P_n)$	$G(s) = -\frac{\Delta W P_n S}{1 + \Delta W P_n}$
$P = P_n / (1 + \Delta W)$	$G(s) = -\frac{\Delta W S}{1 + \Delta W}$

In order to analyze the stability of the equivalent feedback loop shown in Figure 2a, we will assume $r \equiv g \equiv 0$. In Figure 2b, we redraw the $1 + G$ term explicitly with zero external excitations and small gain theorem becomes applicable to the shown loop. It is straightforward to derive $\frac{u_G}{y_G} = -\frac{K}{s+K} = -Q$ and the necessary condition for stability is to choose $\| -Q \|_\infty < 1$, which leads to choosing $K > 0$ if $\|G\|_\infty < 1$. Following remark summarizes the stability conclusion of our discussion.



(a) Expanded Q -filter based disturbance observer block diagram.



(b) Small gain theorem equivalent of the diagram.

Figure 2. Feedback representation from d to \hat{d} and the block diagram for small gain theorem.

Remark 1 If the uncertain transfer function G has no unstable poles and $\|G\|_\infty < 1$ is satisfied, for any $K > 0$, the closed loop system in Figure 2a is stable.

Regarding the final value of $d - \hat{d}$ in Figure 2a, assuming $G(0) > 0$, one can derive the static error constants as $K_p = \lim_{s \rightarrow 0} (1 + G) \frac{K}{s} = \infty$ and $K_v = \lim_{s \rightarrow 0} s(1 + G) \frac{K}{s} = (1 + G(0))K$. Apparently, the larger the value of K the better the disturbance prediction performance for ramp-like disturbances.

Aside from the steady state performance issues, we may write the following matrix equation in between

the output variables $\{\hat{d}, y\}$ and the input variables $\{d, r, g\}$.

$$\begin{bmatrix} \hat{d} \\ y \end{bmatrix} = \underbrace{\begin{bmatrix} \mathcal{A}_{11} & \mathcal{A}_{12} \\ \mathcal{A}_{21} & \mathcal{A}_{22} \end{bmatrix}}_A \begin{bmatrix} d \\ r \end{bmatrix} + \underbrace{\begin{bmatrix} \mathcal{B}_1 \\ \mathcal{B}_2 \end{bmatrix}}_B g \quad (4)$$

where $\mathcal{A}_{11} = \frac{K(1+G)}{s+K(1+G)}$, $\mathcal{A}_{12} = \frac{KGC}{s+K(1+G)}$, $\mathcal{A}_{21} = PS \frac{s}{s+K(1+G)}$, $\mathcal{A}_{22} = T \frac{s+K}{s+K(1+G)}$, $\mathcal{B}_1 = \frac{KN}{s+K(1+G)}$ and $\mathcal{B}_2 = -PS\mathcal{B}_1 - T$.

Assume $g \equiv 0$ and let the error vector be $\epsilon(j\omega) := \begin{bmatrix} d(j\omega) - \hat{d}(j\omega) \\ r(j\omega) - y(j\omega) \end{bmatrix}$ and the independent external excitation be $F(j\omega) := \begin{bmatrix} d(j\omega) \\ r(j\omega) \end{bmatrix}$. With these definitions, we can write the following frequency dependent matrix equation.

$$\begin{bmatrix} d(j\omega) - \hat{d}(j\omega) \\ r(j\omega) - y(j\omega) \end{bmatrix} = (I - \mathcal{A}(j\omega)) \begin{bmatrix} d(j\omega) \\ r(j\omega) \end{bmatrix} \quad (5)$$

The energy of the error vector at frequency ω and that of the independent external excitation are related to each other as follows

$$\epsilon^H \epsilon = F^H \mathcal{M} F \quad (6)$$

where ϵ^H is the conjugate transpose of ϵ and $\mathcal{M} := (I - \mathcal{A})^H (I - \mathcal{A})$ and \mathcal{M} is a Hermitian matrix that is dependent upon the frequency, ω . Rayleigh quotient, which quantifies the energy of the error (ϵ) at frequency ω over the energy of the independent excitation signal (F) at that frequency, can now be defined as

$$\frac{\epsilon^H \epsilon}{F^H F} = \frac{F^H \mathcal{M} F}{F^H F} := R(\mathcal{M}, F) \quad (7)$$

Defining $\lambda_{\min}\{\mathcal{M}\}$ and $\lambda_{\max}\{\mathcal{M}\}$ as the smallest and largest eigenvalues of \mathcal{M} , respectively, one has the following inequality:

$$\lambda_{\min}\{\mathcal{M}\} \leq R(\mathcal{M}, F) \leq \lambda_{\max}\{\mathcal{M}\} \quad (8)$$

Ideally, one wants to have $\mathcal{A} = I_{2 \times 2}$, $\mathcal{M} = 0_{2 \times 2}$ and $\mathcal{B} = 0_{2 \times 1}$ and perfect tracking is observed at every frequency, yet this is not the case in practice and it is desired to have small $\lambda_{\max}\{\mathcal{M}\}$ and the values of the eigenvalues of \mathcal{M} depend upon K , P , G and C . This is seen from the entries of the matrix \mathcal{A} . An acceptable result would be to obtain $|\mathcal{A}_{11}(j\omega)| \approx 1$, $|\mathcal{A}_{22}(j\omega)| \approx 1$, $|\mathcal{A}_{12}(j\omega)| \ll 1$ and $|\mathcal{A}_{21}(j\omega)| \ll 1$ over the bandwidth of the nominal closed loop transfer function, T_n , say $0 \leq \omega \leq \omega_{T_n}$.

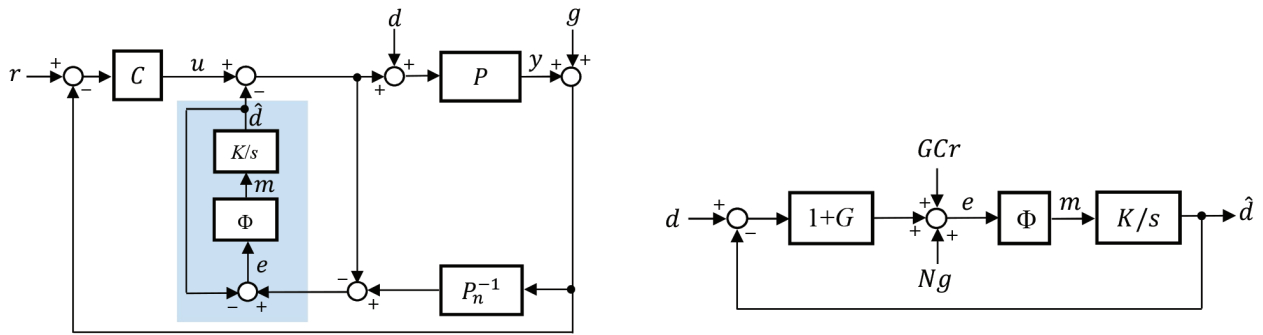
Finally in this section, we present the implications of $\|G\|_\infty < 1$ on the terms seen in the second column of Table. Since $\|\Delta\|_\infty \leq 1$, one needs $\|WS\|_\infty < 1$ for the first type of uncertainty model, $\|P_n^{-1}WS\|_\infty < 1$ for the second type, $\|\frac{P_n WS}{1+\Delta W P_n}\|_\infty < 1$ for the third type and $\|\frac{WS}{1+\Delta W}\|_\infty < 1$ for the last type of uncertainty described in Table.

In the remaining part of this study, we restrict ourselves to the first type of uncertainty, i.e. $P = P_n(1+\Delta W)$ and leave the other uncertainty types to future studies. The stability condition for $P = P_n(1+\Delta W)$

reduces to the well known robust stability condition, $\|WS\|_\infty < 1$. The next section describes the proposed modification for the classical Q -filter based loop and a new discontinuous filter, the S-filter, is introduced and the analytical aspects are discussed.

3. S-filter based enhanced DOBC scheme

In this section, we propose modifying the block diagram of the original DOBC structure by adding the nonlinear function Φ as shown in Figure 3a. The signal to the block K/s was $e(t)$ in the Q -filter configuration, whereas S-filter scheme considers $m(t) = \Phi(e(t))$ as the signal multiplied by K and then integrated to obtain \hat{d} . Using the equations (1) and (2), the equivalent block diagram illustrated in Figure 3b is obtained. The discussion here is to specify the nonlinear function Φ together with the stability conditions and performance limitations.



(a) Block diagram of the S-filter based disturbance observer scheme.

(b) Reorganized block diagram of the S-filter based disturbance observer scheme, which can detect small magnitude matched disturbances.

Figure 3. Proposed DOBC structure and its equivalent representation.

The nonlinear function considered in this paper is a signum function, i.e. $\Phi(e(t)) := \text{sgn}(e(t))$, which is sensitive to small magnitude disturbances and we call the corresponding subsystem as S-filter. In the sequel, we study the stability properties of the loop shown in Figure 3b by setting $r \equiv g \equiv 0$.

Consider the Lyapunov function candidate $V = \frac{1}{2}e^2$ and define the impulse response of the term $G(s)$ as $\tilde{g}(t)$. According to the figure,

$$e = (d - \hat{d}) + \tilde{g} \star (d - \hat{d}) \tag{9}$$

where \star denotes the convolution operation, which lets us write $\dot{e} = (\dot{d} - \dot{\hat{d}}) + \tilde{g} \star (\dot{d} - \dot{\hat{d}})$. Further, according to Figure 3a, we have

$$\dot{\hat{d}} = K \text{sgn}(e) \tag{10}$$

Therefore,

$$\dot{e} = (\dot{d} - K \text{sgn}(e)) + \tilde{g} \star (\dot{d} - K \text{sgn}(e)) \tag{11}$$

The time derivative of V can now be written and rearranged as below.

$$\dot{V} = e\dot{e} \quad (12)$$

$$= (\dot{d} + \tilde{g} \star \dot{d})e - K|e| - K(\tilde{g} \star \text{sgn}(e))e \quad (13)$$

$$= (\dot{d} + \tilde{g} \star \dot{d})e - K|e| - K(\tilde{g} \star 1)e \text{sgn}(e) \quad (14)$$

$$\leq (\dot{d} + \tilde{g} \star \dot{d})e - K|e| + K\|\tilde{g}\|_1|e| \quad (15)$$

$$= f(t)e - K(1 - \|\tilde{g}\|_1)|e| \quad (16)$$

where $f(t) := \dot{d} + \tilde{g} \star \dot{d}$.

Assuming $|\dot{d}(t)| \leq \mathcal{B}_d$, using the definition of the convolution, we have

$$\dot{d} + \tilde{g} \star \dot{d} = \dot{d} + \int_0^t \tilde{g}(t - \tau)\dot{d}(\tau)d\tau \quad (17)$$

$$\leq \mathcal{B}_d + \int_0^t |\tilde{g}(t - \tau)||\dot{d}(\tau)|d\tau \quad (18)$$

$$\leq \mathcal{B}_d + \mathcal{B}_d \int_0^t |\tilde{g}(t - \tau)|d\tau \quad (19)$$

$$\leq \mathcal{B}_d + \mathcal{B}_d(\|\tilde{g}\|_1) \quad (20)$$

$$= \mathcal{B}_d(1 + \|\tilde{g}\|_1) \quad (21)$$

According to (21), $|f(t)| \leq \mathcal{B}_d(1 + \|\tilde{g}\|_1)$, this would let us continue (16) as

$$\dot{V} \leq |f(t)||e| - K(1 - \|\tilde{g}\|_1)|e| \quad (22)$$

$$\leq \mathcal{B}_d(1 + \|\tilde{g}\|_1)|e| - K(1 - \|\tilde{g}\|_1)|e| \quad (23)$$

$$= (\mathcal{B}_d(1 + \|\tilde{g}\|_1) - K(1 - \|\tilde{g}\|_1))|e| \quad (24)$$

If $K > \mathcal{B}_d \frac{1 + \|\tilde{g}\|_1}{1 - \|\tilde{g}\|_1}$ and $\|\tilde{g}\|_1 < 1$, then the loop shown in Figure 3b is Lyapunov stable.

Remark 2 The very role of the nonlinear term here is to increase the loop gain when the input variable e in Figs. 3a-3b is close to zero, and this makes the proposed mechanism sensitive to small e values and the necessary corrective action on \hat{d} can be taken appropriately.

Now consider the Fourier transform of \tilde{g} , i.e. $\mathcal{F}\{\tilde{g}\} = G(j\omega)$ and we can write the magnitude of this as $|G(j\omega)| = |\int_0^\infty \tilde{g}(t)e^{-j\omega t}dt| \leq \int_0^\infty |\tilde{g}(t)||e^{-j\omega t}|dt \leq \int_0^\infty |\tilde{g}(t)|dt = \|\tilde{g}\|_1$. This result above naturally leads to $\|G\|_\infty \leq \|\tilde{g}\|_1$. Since we require $\|\tilde{g}\|_1 < 1$ and $K > \mathcal{B}_d \frac{1 + \|\tilde{g}\|_1}{1 - \|\tilde{g}\|_1}$, the closed loop system in Figure 3b will be robustly stable under the presence of uncertainties satisfying $\|\tilde{g}\|_1 < 1$.

In summary, it is common to have $K > \mathcal{B}_d$ in both Q-filter and S-filter approaches, Q-filter approach needs $\|G\|_\infty < 1$ as the second condition and S-filter based approach needs $\|\tilde{g}\|_1 < 1$. Since $\|G\|_\infty \leq \|\tilde{g}\|_1$, the latter addresses a larger set of uncertainties.

The question at this point is the performance comparison of the system in Figure 3b for the cases of Q -filter adopting $\Phi(e) = e$ and the proposed S-filter that uses $\Phi(e) = \text{sgn}(e)$. The closed loop transfer function from d to \hat{d} when $g \equiv r \equiv 0$ is equal to

$$T_Q(s) = \frac{K(1 + G(s))}{s + K(1 + G(s))} \tag{25}$$

while the quasi linear representation of the nonlinear element Φ lets us have

$$T_S(s) = \frac{\frac{4K}{\pi A^*}(1 + G(s))}{s + \frac{4K}{\pi A^*}(1 + G(s))} \tag{26}$$

where A^* denotes the magnitude of oscillations at the input of the nonlinear element, i.e. the signum function. For the same $G(s)$ and K , the magnitude of oscillations become effective in the bandwidth of the closed loop system. It is evident from (26) that for small magnitude oscillations satisfying $A^* < \frac{4}{\pi}$, the bandwidth is higher than the Q -filter based DOBC scheme and the disturbance prediction performance of the S-filter based approach is visibly better than the classical DOBC scheme.

In order to understand the enhancement of the bandwidth, define

$$\gamma_L := \inf_{\omega \in \mathbb{R}} |1 + G(j\omega)| \tag{27}$$

$$\gamma_U := \sup_{\omega \in \mathbb{R}} |1 + G(j\omega)| \tag{28}$$

Since $\|G\|_\infty < 1$, we have $\gamma_U < 2$. With the above definitions, we can write $\gamma_L \leq |1 + G(j\omega)| \leq \gamma_U$. The bandwidth of the transfer function in (25) is obtained from the solution of

$$\omega_{bw} = K|1 + G(j\omega_{bw})| \tag{29}$$

For the transfer function in (25), the equality above lets us have

$$K\gamma_L \leq \omega_{bw} \leq K\gamma_U \tag{30}$$

A similar approach would produce the following range for the transfer function in (26).

$$\frac{4}{\pi A^*} K\gamma_L \leq \omega_{bw} \leq \frac{4}{\pi A^*} K\gamma_U \tag{31}$$

Comparing the two inequalities and considering the conformal map property of Nyquist plots, since $A^* < \frac{4}{\pi}$, the bandwidth of the S-filter based approach will be wider than the Q -filter based approach.

Lastly, in this section, we will compare the energies of the disturbance prediction errors, $d - \hat{d}$ for the Q -filter and S-filter cases. Define the energy of the error signal in time domain as

$$\mathcal{E} := \sqrt{\int_0^\infty (d - \hat{d})^2 dt} = \sqrt{\frac{1}{2\pi} \int_{-\infty}^\infty |d(j\omega) - \hat{d}(j\omega)|^2 d\omega} \tag{32}$$

where the right hand side is due to the Parseval's theorem. We will denote the energy equation obtained for the Q -filter by \mathcal{E}_Q and that for the S-filter by \mathcal{E}_S and proceed considering the quasi linear regime conditions by writing the following expressions.

$$\mathcal{E}_Q^2 = \frac{1}{2\pi} \int_{-\infty}^{\infty} \frac{|d(j\omega)|^2}{\left|1 + (1 + G(j\omega))\frac{K}{j\omega}\right|^2} d\omega = \frac{1}{2\pi} \int_{-\infty}^{\infty} \frac{\omega^2 |d(j\omega)|^2}{|j\omega + (1 + G(j\omega))K|^2} d\omega \tag{33}$$

$$\mathcal{E}_S^2 = \frac{1}{2\pi} \int_{-\infty}^{\infty} \frac{|d(j\omega)|^2}{\left|1 + (1 + G(j\omega))\frac{4K}{\pi A^*}\right|^2} d\omega = \frac{1}{2\pi} \int_{-\infty}^{\infty} \frac{\omega^2 |d(j\omega)|^2}{\left|j\omega + (1 + G(j\omega))\frac{4K}{\pi A^*}\right|^2} d\omega \tag{34}$$

To be able to compare the two energy expressions, consider Figure 4, where the shaded area in top left drawing indicate the possible subspace for $G(j\omega)$ as $\|G\|_{\infty} < 1$. The shaded area in the bottom left subplot depicts set of all locations for the quantity $1 + G(j\omega)$. The right subplot depicts two colored circles, the small one is for the quantity $j\omega + K(1 + G)$ and the large one is for $j\omega + \frac{4K}{\pi A^*}$. Clearly since $A^* < \frac{4}{\pi}$, the radii satisfy $\frac{4K}{\pi A^*} > K$ and the S-filter creates the larger circle. The lines drawn from the origin are denoted by l_Q and l_S and these values correspond to the distances seen in the denominators of the integrands in (33) and (34). Depending on the value of A^* , and the considered frequency value, ω , S-filter generates much larger distances than the Q -filter for small magnitude oscillations. This is visible as one starts from $\omega = 0$ in Figure 4 and runs toward infinity.

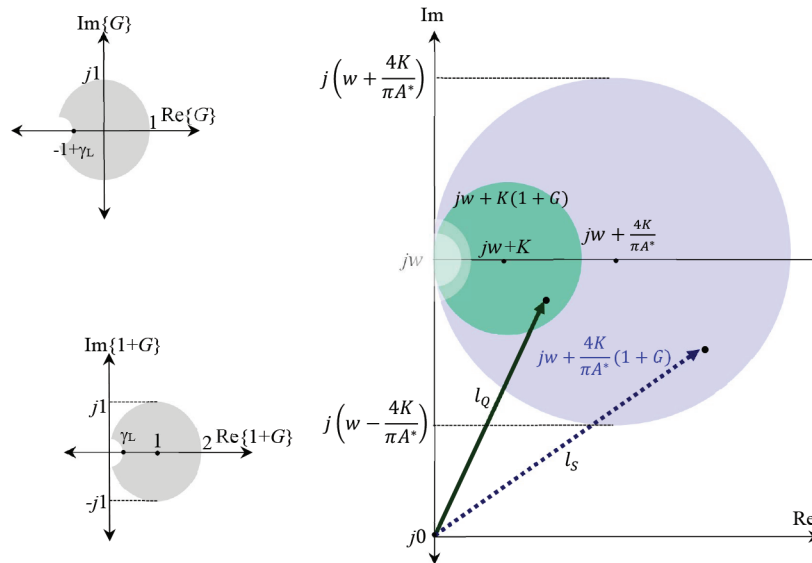


Figure 4. Comparison of the denominators of (33) and (34) in complex plane.

As a last issue in this part, we will discuss the transient performance of the two schemes comparatively. Consider Figure 3b for the nominal case, i.e. $\Delta \equiv 0$ ($G \equiv 0$) and no noise, i.e. $g \equiv 0$. According to the figure, we read the error as $e = d - \hat{d}$. The diagram produces S-filter scheme when $\Phi(e(t)) = \text{sgn}(e(t))$. For this case, we will denote $e_S(t)$ as the error seen in the figure. Similarly, if $e(t) \equiv m(t)$, i.e. there is no nonlinear element,

then we obtain Q -filter case and we denote error seen in the loop by $e_Q(t)$. For the S-filter configuration, it is possible to write the following.

$$\dot{e}_S = \dot{d} - K \operatorname{sgn}(e_S) \quad (35)$$

Since we consider the describing function explanation, we set $d(t) := A_d \sin(\omega t)$, where ω is the frequency and A_d is the magnitude of the sinusoidal excitation. This leads to

$$\dot{e}_S = A_d \omega \cos(\omega t) - K \operatorname{sgn}(e_S) \quad (36)$$

Now we will assume $e_S(0) > 0$ initially and integrate the expression above. Note that it is easy to do the same for $e_S(0) < 0$. Since $e_S(0) > 0$, $\operatorname{sgn}(e_S) = 1$ till $e_S(t_h) = 0$ is reached and we will integrate till the hitting time (t_h) at which $e_S = 0$ is reached. This yields

$$\int_0^{t_h} \dot{e}_S(\tau) d\tau = \int_0^{t_h} A_d \omega \cos(\omega \tau) d\tau - K \int_0^{t_h} d\tau \quad (37)$$

Taking the integral produces

$$e_S(t_h) - e_S(0) = A_d \sin(\omega t)|_0^{t_h} - K t_h \quad (38)$$

Clearly $e_S(t_h) = 0$ and we have

$$t_h = \frac{e_S(0) + A_d \sin(\omega t_h)}{K} \leq \frac{|e_S(0)| + A_d |\sin(\omega t_h)|}{K} \leq \frac{|e_S(0)| + A_d}{K} \quad (39)$$

Following the same steps for when $e_S(0) < 0$ will result in the same bound, i.e. the time required to reach $e_S(t_h) = 0$ is bounded and it is given by $t_h \leq \frac{|e_S(0)| + A_d}{K}$.

On the other hand, for the Q -filter case, we have $\dot{d} = K e_Q$. Solving this differential equation for $d(t) = A_d \sin(\omega t)$, we obtain the following equality for t_h .

$$\left(\hat{d}(0) + A_d \frac{K \omega}{K^2 + \omega^2} \right) e^{-K t_h} - \frac{\omega^2 A_d}{K^2 + \omega^2} \sin(\omega t_h) - \frac{K A_d}{K^2 + \omega^2} \omega \cos(\omega t_h) = 0 \quad (40)$$

Looking at (40), since the solution at $t = t_h$ produce a nonlinear equation in the parameters, we present a number of exemplar cases. Further, Q -filter case generates exponential convergence, so t_h may not even be computable yet the convergence may favor Q -filter for some initial conditions or some disturbance magnitudes. Therefore, we study a number of simulations to see whether one approach is consistently performing good or not.

As we consider $K = 100$ in this work, in the simulations below, we keep this value and change the initial conditions. We consider a sinusoidal disturbance with frequency $\omega = 20$ rad/s and considered magnitudes equal to 1 and 5. Several initial conditions are studied and We illustrate one period of the results in Figs. 5a-5b.

As seen from the results in Figs. 5a-5b, transient responses do not recommend one or the other approach consistently. This work claims when $A^* < 4/\pi \approx 1.2732$, after the transient phase, S-filter is the good choice if the prescribed conditions are met. The simulations display no visible fluctuations in the error response of the S-filter approach.

In the next section, we provide a comparative work to prove the theoretical claims presented here.

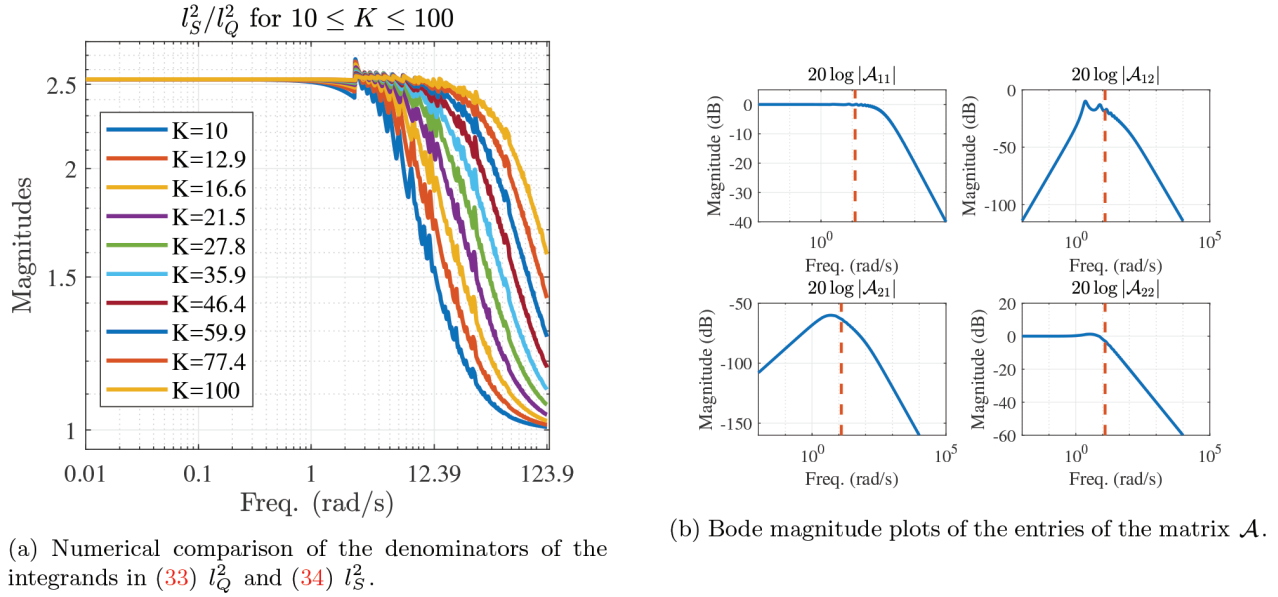


Figure 5. Comparison of the transient performances of the two schemes.

4. Simulation studies: a comparison of Q -filter and S -filter based DOs

Let the nominal plant model $P_n = \frac{1}{s^2}$ and the nominal unity feedback control loop has a proportional plus derivative (PD) controller given as $C = k_p + k_d s$. In the initial set of simulations, we will consider $\Delta = e^{-\tau s}$, which is a time delay of τ seconds and $W = \frac{a}{s+a}$. With these definitions, the uncertain plant has the transfer function $P = P_n(1 + \Delta W) = (1 + e^{-\tau s} \frac{a}{s+a}) \frac{1}{s^2}$.

In the comparison work we carried out, $k_p = 25$ and $k_d = 10$, which results in a nominal control system with bandwidth $\omega_{T_n} = 12.39$ rad/s. For these values, we perform a grid search over logarithmic spaced 1000 frequencies $\omega \in [0.001, 10\omega_{T_n}]$, 10 linearly spaced delay values (τ) in between 0 and 1, and logarithmic spaced 100 points for $A^* \in [0.001, 0.8]$. The results for this search are illustrated in Figure ??a, where we see the ratio l_S^2/l_Q^2 ($l_Q(j\omega) := |j\omega + (1 + G(j\omega))K|^2$ and $l_S(j\omega) := |j\omega + (1 + G(j\omega)) \frac{4K}{\pi A^*}|^2$) for different K values. We consider logarithmic spaced ten K values in between 10 and 100 and record the worst observed value of l_S^2/l_Q^2 . For all curves, compared to Q -filter approach, it is clear that the proposed approach generates larger denominator, i.e. $l_S^2 > l_Q^2$, leading to smaller energy for the error signal, $d - \hat{d}$.

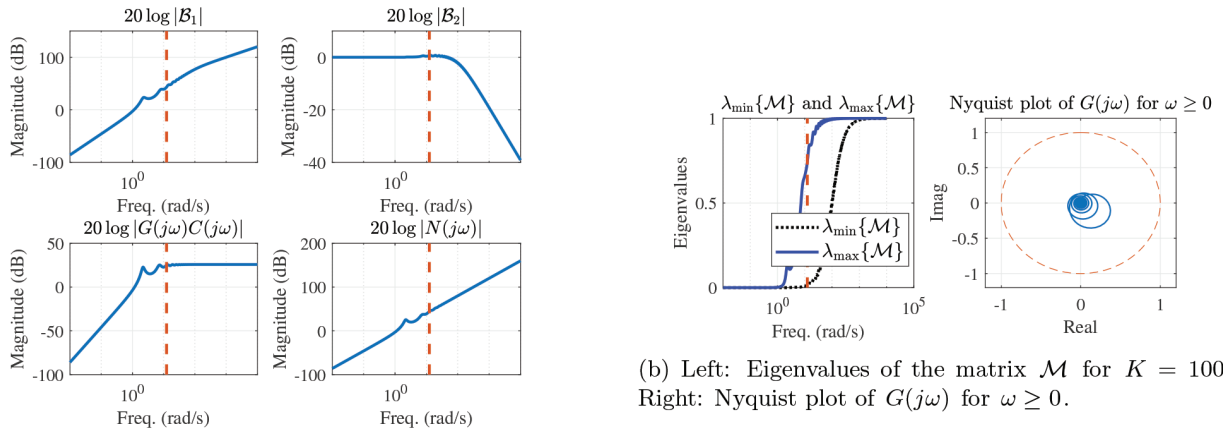
In the simulations, we consider $a = 3$ and $\tau = 1$ s, which leads to $G(s) = e^{-s}(\frac{3}{s+3})(\frac{1}{1+P(s)(10s+25)})$, where $P(s) = (1 + \frac{3}{s+3}e^{-s})\frac{1}{s^2}$. These selections ensure $\|\Delta\|_\infty \leq 1$, $\|G\|_\infty < 1$ and $\|\hat{g}\|_1 < 1$. For these selections, we observe $\gamma_L = 0.7957$. Exact signum function is used without any smoothing.

In Fig ??b, we illustrate the subplots of the matrix \mathcal{A} in (4). The figure is drawn for $K = 100$ and as expected, it is seen that $|\mathcal{A}_{11}|$ and $|\mathcal{A}_{22}|$ have a lowpass characteristic with low frequency gain equal to 0 dB. The off-diagonal terms of the matrix \mathcal{A} are not zero, yet they are fairly suppressed in the low frequency range. The peak gain of $|\mathcal{A}_{21}|$ is nearly -60 dB and the output is almost completely decoupled from the disturbance signal. The term $|\mathcal{A}_{12}|$ is small in the low frequency range and it climbs up to 26.6 dB as the frequency increases

then starts decreasing for the rightmost part of the ω axis. A natural consequence of this is to observe the effect of the high frequency components of the command signal on \hat{d} . This will have some influence over the performance of the Q -filter based DOBC scheme. Since the change in S-filter approach is to introduce an infinite gain limiter into the path, we expect a similar effect in S-filter approach yet with smaller disturbance prediction error energy compared to the Q -filter approach. The frequency ω_{T_n} is shown as a dashed vertical line in all subplots for better understanding of the Bode plots.

Figure 6a depicts the Bode magnitude plots of the matrix \mathcal{B} of (4) and those of $G(j\omega)C(j\omega)$ and $N(j\omega)$ of (3). Clearly, both terms have limited effect on the performance for low frequencies; however, as the frequency increases, the degradation in the disturbance prediction performance increases and both approaches display poor performances.

The eigenvalues of the matrix \mathcal{M} and the Bode plot of $G(j\omega)$ are shown in Figure 6b, where it is seen that an increase in the frequency provokes the coupling effect within (r, \hat{d}) and (y, d) pairs and both approaches function properly for slowly changing disturbance signals.



(a) Bode magnitude plots of the entries of the matrix \mathcal{B} and those of $G(j\omega)C(j\omega)$ and $N(j\omega)$.

Figure 6. Effect of the value of gain K and $20 \log |\mathcal{A}|$ over the frequency axis.

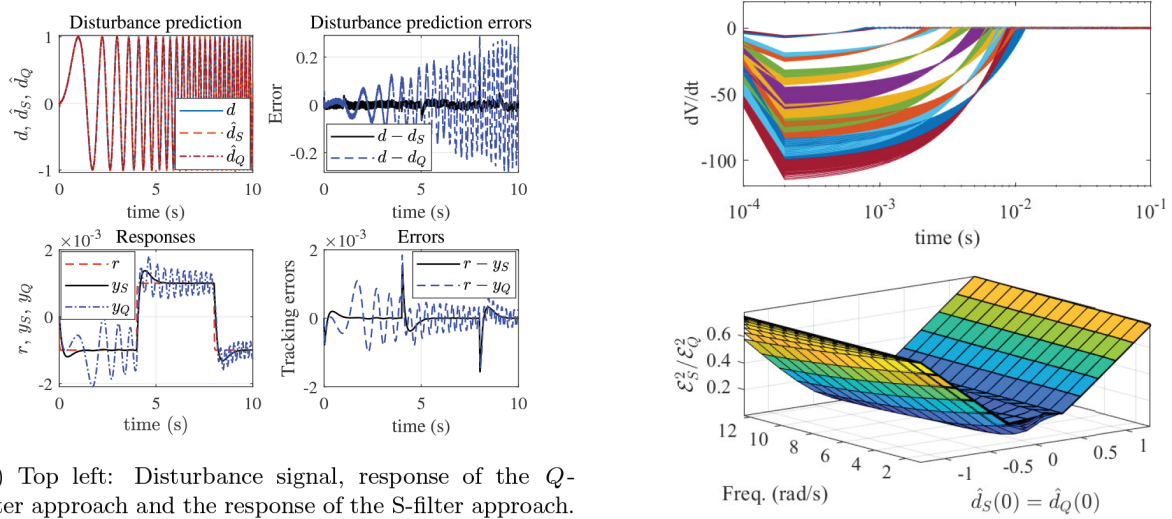
Time domain test results are presented in Figure 7a, where the disturbance signal is a chirp signal with initial frequency 0.01 rad/s and the final frequency is 12.39 rad/s, which is equal to ω_{T_n} . Output measurements are slightly noisy and a noise signal (g) having uniform distribution over $\pm 1e-8$ is added to the output variable y .

The top left subplot of Figure 7a depicts d , together with the predictions for Q -filter denoted by \hat{d}_Q and those for the S-filter, denoted by \hat{d}_S . The top right subplot demonstrates the quantities $d - \hat{d}_Q$ (dashed blue) and $d - \hat{d}_S$ (solid black). The proposed scheme consistently produces much lower errors as the frequency increases. The reference signal has deliberately been chosen as a square wave signal to show how S-filter based approach outperforms the standard scheme. The bottom left and right subplots of Figure 7a illustrate the outputs and output tracking error trends, respectively. In these subplots, the superiority of the proposed S-filter based approach is seen clearly. Since the command signal varies in between $\pm 1e-3$, we deliberately chose a noise signal varying within a narrow range. As the noise magnitude is increases, the performances for both

approaches deteriorate gradually.

Looking at the disturbance prediction performances shown in Figure 7a, the delay on \hat{d}_Q is larger than that on \hat{d}_S and this makes the disturbance prediction error to rise up to magnitudes close to 0.3 on the top right subplot. This is particularly effective when the disturbance signal has fast fluctuations and the proposed technique maintains the prediction performance over a wider spectrum than Q -filter based approach. This is a clear evidence of the benefit of using the S-filter based DOBC scheme.

Next, we consider the time derivative of the Lyapunov function in (12), for an exhaustive search considering $r(t) = A \sin(\omega t)$ and 14 linearly spaced points for the initial conditions satisfying $-1 \leq \hat{d}_Q(0) = \hat{d}_S(0) \leq 1$, ten logarithmic points for the magnitude A satisfying $0.01 \leq A \leq \frac{4}{\pi}$, 15 logarithmic spaced points for $\omega \in \{1, \omega_{T_n}\}$ rad/s. The results for the \dot{V} are shown on the top subplot and the results comparing the energy of $d - \hat{d}_Q$ and $d - \hat{d}_S$ for 0.1 s of simulation are depicted in the bottom subplot of Figure 7b. We plot $\mathcal{E}_S^2/\mathcal{E}_Q^2$ and expect to see a family of surfaces that is less than 0.7 in all points and the results on the figure support this claim. Each value of the variable A produces an individual surface sheet in the figure.



(a) Top left: Disturbance signal, response of the Q -filter approach and the response of the S-filter approach. Top right: Disturbance prediction errors. Bottom left: Reference signal and the outputs for Q -filter and S-filter cases. Bottom right: Output tracking errors.

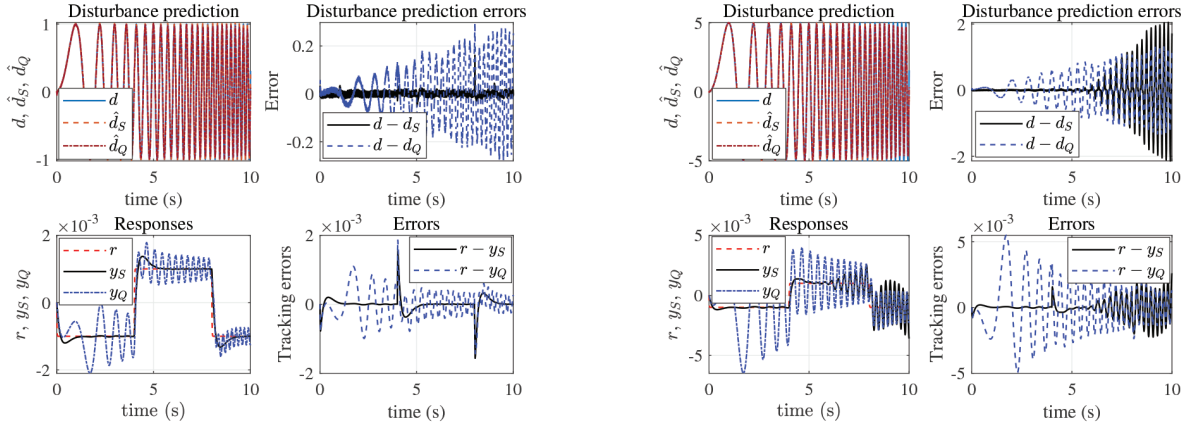
(b) $r(t) = A \sin(\omega t)$ and $-1 \leq \hat{d}_Q(0) = \hat{d}_S(0) \leq 1$, $0.01 \leq A \leq \frac{4}{\pi}$, $\omega \in \{1, \omega_{T_n}\}$ rad/sec. Top: $\dot{V}(t)$. Bottom: $\mathcal{E}_S^2/\mathcal{E}_Q^2$ for $0 \leq t \leq 1$ sec.

Figure 7. Spectral properties of the proposed scheme, eigenvalues of \mathcal{M} and the Nyquist plot of G .

Lastly, we consider dynamic uncertainty case where $\Delta = e^{-s} \frac{s^2+10}{s^2+8s+10}$ and re-simulate the feedback loops for the unity magnitude chirp signal in Figure 8a and a chirp with magnitude equals to five in Figure 8b. In Figure 8a, we see that the tracking errors and the disturbance prediction errors for the proposed scheme is better than the Q -filter case. Proposed scheme generates smoother output tracking performance that displays almost no interference with the chirp disturbance. This is clear from the top right subplot of Figure 8a, where the disturbance prediction error of the S-filter mechanism is maintained very close to zero.

In Figure 8b, we multiply the disturbance magnitude by 5 and see that after $t \approx 6.45$ s. the performances of both approaches get poorer and $t \approx 6.45$ s is the time after which $K > \mathcal{B}_i$ is violated. The chosen K value

satisfies $100 = K > \mathcal{B}_d \frac{1+\|\tilde{g}\|_1}{1-\|\tilde{g}\|_1} = 94.7$ for our simulations and the obtained results justify our claims. If $K > \mathcal{B}_d$ is violated, the deterioration in the performance of the S-filter is quicker than that of the Q-filter.



(a) Results when disturbance magnitude is unity. Top left: Disturbance signal, response of the Q -filter approach and the response of the S -filter approach. Top right: Disturbance prediction errors. Bottom left: Reference signal and the outputs for Q -filter and S -filter cases. Bottom right: Output tracking errors.

(b) Results when disturbance magnitude is 5. Top left: Disturbance signal, response of the Q -filter approach and the response of the S -filter approach. Top right: Disturbance prediction errors. Bottom left: Reference signal and the outputs for Q -filter and S -filter cases. Bottom right: Output tracking errors.

Figure 8. Simulation results with pure delay

5. Contributions of the S-Filter approach

- Converting Figure 1a to Figure 1b is a useful interpretation of DOBC scheme, [31], as the new block diagram lets us obtain a feedback loop in Figure 2a showing $GCr + Ng$ term as the load disturbance and the primary loop has d as the command input and \hat{d} as the output. Figure 2a is an implementation of equation (3).
- This representation yields the fundamental equation given in (3), which is valid for all uncertainty models tabulated in the Table. A natural consequence of (3) is the equation (4) and the result of this is (8).
- Inserting a signum function as in Figure 3a is a novel approach making the disturbance prediction loop nonlinear and this lets us obtain the equivalent loop shown in Figure 3b.
- The analysis of the classical DOBC scheme and the proposed scheme has produced $K > \mathcal{B}_d \frac{1+\|\tilde{g}\|_1}{1-\|\tilde{g}\|_1}$ and $\|G\|_\infty < 1$. The proposed approach requires $\|\tilde{g}\|_1 < 1$ for stability. Discrete time version of the same block structure requires $\|\tilde{g}_k\|_1 < 1/2$ for stability. Here, \tilde{g}_k represents the impulse response of the corresponding quantity in [30].
- The comparisons in terms of the \mathcal{L}_2 norms of the disturbance prediction errors are the issues strengthening the novelties.
- The proposed method enhances the reference signal tracking performance making the proposed technique a candidate for precise positioning systems involving uncertainty and imprecision.

6. Conclusion

This paper introduces a modification to the classical Q -filter based DOBC scheme. Unlike the classical scheme, which considers the Q -filter as a transfer function, the filter structure is implemented in feedback form and the proposed modification is made into it, yielding a nonlinear filter. The proposed modification makes the obtained disturbance observer sensitive to small magnitude matched disturbance signals. Although the transient responses do not recommend the same approach consistently, S-filter approach improves the steady regime performance of the closed loop system significantly. Spectral properties and the time domain performances are discussed comparatively and the energies of the resulting disturbance prediction errors are compared. The results show that the proposed approach enhances the classical Q -filter based DOBC scheme under certain conditions.

References

- [1] Ohishi K, Ohnishi K, Miyachi K. Torque-speed regulation of dc motor based on load torque estimation method. In: Proceedings of the JIEE International Power Electronics Conference; Tokyo, Japan; 1983. pp.1209-1218.
- [2] Sarıyıldız E, Ohnishi K. A guide to design disturbance observer. ASME Journal of Dynamic Systems, Measurement and Control 2014. 136: Art.ID:021011.
- [3] Sarıyıldız E, Ohnishi K. Stability and robustness of disturbance-Observer-based motion control systems. IEEE Transactions on Industrial Electronics 2015; 62 (1): 414-422.
- [4] Sarıyıldız E, Sekiguchi H, Nozaki T, Ugurlu B, Ohnishi K. A stability analysis for the acceleration-based robust position control of robot manipulators via disturbance observer. IEEE/ASME Transactions on Mechatronics 2018; 23 (5): 2369-2378.
- [5] Sarıyıldız E, Ohnishi K. Bandwidth constraints of disturbance observer in the presence of real parametric uncertainties. European Journal of Control 2013; 19: 199-205.
- [6] Sarıyıldız E, Ohnishi K. Performance and robustness trade-off in disturbance observer design. In: 39th Annual Conference of the IEEE Industrial Electronics Society; Vienna, Austria; 2013. pp.3681-3686.
- [7] Sarıyıldız E, Ohnishi K. Design constraints of disturbance observer in the presence of time delay. In: IEEE International Conference on Mechatronics; Vicenza, Italy 2013. pp.69-74.
- [8] Sarıyıldız E, Ohnishi K. Analysis the robustness of control systems based on disturbance observer. International Journal of Control 2013; 86 (10): 1733-1743.
- [9] Chang H, Kim H, Park G, Shim H. Do-dat: a matlab toolbox for design & analysis of disturbance observer. In: IFAC-PapersOnLine; 2018, 51 (25): 340-345.
- [10] Schrijver E, van Dijk J. Disturbance observers for rigid mechanical systems: equivalence, stability, and design. ASME Journal of Dynamic Systems, Measurement and Control 2002; 124: 539-548.
- [11] Wang CC, Tomizuka M. Design of robustly stable disturbance observers based on closed loop consideration using H_∞ optimization and its applications to motion control systems. In: Proceedings of the 2004 American Control Conference; Boston, MA, USA; 2004. pp.3764-3769.
- [12] El-Shaer AH, Tomizuka M. Robust tracking performance and disturbance rejection for a class of nonlinear systems using disturbance observers. In: Proceedings of the American Control Conference; Washington DC, USA; 2013. pp.1082-1087.
- [13] Ali H, Ali A, Shaikh IUH. Disturbance observer based control of twin rotor aerodynamic system. Turkish Journal of Electrical Engineering & Computer Sciences 2020; 28: 2213-2227.
- [14] Li SH, Yang J, Chen WH, Chen XS. Disturbance Observer Based Control: Methods and Applications. Boca Raton, FL, USA: CRC Press, 2014.

- [15] Chen WH, Yang J, Guo L, Li S. Disturbance-observer-based control and related methods-an overview. *IEEE Transactions on Industrial Electronics* 2016; 63 (2): 1083-1095.
- [16] Chen WH. Disturbance observer based control for nonlinear systems. *IEEE/ASME Transactions on Mechatronics* 2004; 9 (4): 706-710.
- [17] Shim H, Jo NH. An almost necessary and sufficient condition for robust stability of closed-loop systems with disturbance observer. *Automatica* 2009; 45 (1): 296-299.
- [18] Li X, Chen SL, Teo CS, Tan KK. Enhanced sensitivity shaping by data-based tuning of disturbance observer with non-binomial filter. *ISA Transactions* 2019; 85: 284-292.
- [19] Sariyıldız E, Oboe R, Ohnishi K. Disturbance observer-based robust control and its applications: 35th anniversary overview. *IEEE Transactions on Industrial Electronics* 2019; 67 (3): 2042-2053.
- [20] Chen X, Komada S, Fukuda T. Design of a nonlinear disturbance observer. *IEEE Transactions on Industrial Electronics* 2000; 47 (2): 429-437.
- [21] Chen WH, Guo L. Analysis of disturbance observer based control for nonlinear systems under disturbances with bounded variation. In: *Control 2004*, University of Bath, UK, 2004. Art.ID: 048.
- [22] Back J, Shim H. Adding robustness to nominal output-feedback controllers for uncertain nonlinear systems: a nonlinear version of disturbance observer. *Automatica* 2008; 44: 2528-2537.
- [23] Kim SK, Ahn CK. Self-tuning proportional-type performance recovery property output voltage-tracking algorithm for dc-dc boost converter. *IEEE Transactions on Industrial Electronics* 2019; 66 (4): 3167-3175.
- [24] Lou G, Gu W, Wang J, Wang J, Gu B. A unified control scheme based on a disturbance observer for seamless transition operation of inverter-interfaced distributed generation. *IEEE Transactions on Smart Grid* 2018; 9 (5): 5444-5454.
- [25] Ja G, Jo NH, Eun Y. Performance degradation due to measurement noise in control systems with disturbance observers and saturating actuators. *Journal of The Franklin Institute-Engineering and Applied Mathematics* 2019; 356: 3922-3947.
- [26] Masud N, Smith C, Isaksson M. Disturbance observer based dynamic load torque compensator for assistive exoskeletons. *Mechatronics* 2018; 54: 78-93.
- [27] Wang L, Liu X, Wang C. Improved disturbance observer based control for airborne photoelectric stabilized platform. *Optik* 2019; 188: 133-136.
- [28] Garrido R, Luna JL. On the equivalence between pd+dob and pid controllers applied to servo drives. In: *IFAC-PapersOnline*; 2018, 51 (4): 95-100.
- [29] Pinagapani AK, Mani G, Chandaran KR, Pandian K. Composite disturbance rejection control for ball balancer system. *Procedis Computer Science* 2018; 133: 124-133.
- [30] Efe MÖ, Kasnakoglu C. A nonlinear disturbance observer scheme for discrete time control systems. *Turkish Journal of Electrical Engineering and Computer Sciences* 2021; DOI: 10.3906/elk-2005-206.
- [31] Uzunovic T, Sariyıldız E, Sabanovic A. A discussion on discrete implementation of disturbance-observer-based control. In: *2018 IEEE 15th International Workshop on Advanced Motion Control*; Tokyo, Japan; 2018. pp.613-618.